ISSN 0023-1584, Kinetics and Catalysis, 2009, Vol. 50, No. 1, pp. 73–81. © Pleiades Publishing, Ltd., 2009.
Original Russian Text © Yu.K. Karasevich, 2009, published in Kinetika i Kataliz, 2009, Vol. 50, No. 1, pp. 80–89.

Kinetics of Chemical Ionization in Shock Waves: II. Kinetic Model of Ionization in Methane Oxidation

Yu. K. Karasevich

Semenov Institute of Chemical Physics, Russian Academy of Sciences, Moscow, 119991 Russia
e-mail: yukarasevich@yandex.ru

Received September 28, 2007

Abstract—A kinetic model is suggested for chemical ionization in methane combustion. The model is based on the view that the primary ionization event in combustion is the associative ionization reaction $CH + O \rightleftharpoons CHO^+ + e^-$. The results of numerical calculations of the ionization kinetics provide a qualitative description for the time variation of the electron concentration. The calculated dependences of the characteristic times, ionization rate, and electron yield on temperature and on the initial methane concentration fit the respective experimental dependences well.

DOI: 10.1134/S0023158409010108

The phenomenon of chemical ionization in flames, that is, the formation of ions via chemical reactions between electroneutral substances, was discovered in the late 1940s [1, 2]. In order to understand the mechanism of chemical ionization, first of all it was necessary to find out what ion appears first. Numerous studies of the ionic composition of flames were carried out for this purpose [3, 4]. As a result, about 50 positive ions were identified. Eventually, it was established that the mechanism of chemical ionization in hydrocarbon flames is based on the following sequence of reactions [5, 6]:

$$CH + O \rightleftharpoons CHO^+ + e^-, \quad \text{(I)}$$

$$CHO^+ + H_2O \rightleftharpoons H_3O^+ + CO, \quad \text{(II)}$$

$$H_3O^+ + e^- \longrightarrow H_2O + H. \quad \text{(III)}$$

In this mechanism, the primary reaction yielding ions in flames is associative ionization (I). Reaction (I) is nearly thermally neutral (ΔH = 4 kcal/mol) [7]. Fast proton transfer to water (reaction (II)) accounts for the presence of H_3O^+, which is the most abundant ion in flames under all reaction conditions.

The rate constants reported in the literature for reactions (II) and (III) are in comparatively good agreement. For example, the rate constant of reaction (II) in flames is estimated at ~7×10^{-9} cm^3/s and it differs from the same rate constant determined experimentally at room temperature, 3.2×10^{-9} cm^3/s [9], only by a small factor of ~2. The rate of the dissociative recombination reaction (III) was measured in many studies, and the results of these measurements are in satisfactory agreement, varying between 1.5×10^{-7} cm^3/s [10] and 4.1×10^{-7} cm^3/s [11]. As for the rate constant of reaction (I), most of the data available from the literature are estimates and these estimates are widely divergent. For example, according to theoretical calculations by MacGregor and Barry [12], the most likely value of this rate constant is 3.5×10^{-11} cm^3/s, while the same rate constant measured by Peeters and Vinckier [13] between 2000 and 2400 K is 2.8×10^{-13} cm^3/s, which is more than 2 orders of magnitude smaller than the calculated value.

There have been only a few reports on the numerical simulation of chemical ionization. Basevich et al. [14] used the methane combustion scheme [15] supplemented by CH radical formation and decay reactions and by reactions (I)–(III) and achieved good agreement with experimental data [16] with respect to one parameter, specifically, the highest concentration of charged species. Numerical simulation was also performed to account for the ionization kinetic data obtained by the probe method for methane oxidation in reflected shock waves [17]. Both the experimental and calculated data obtained in [17] are at variance with the results obtained in the other studies of hydrocarbon ionization. This was a consequence of incorrect use of the probe method.

In an earlier work [18], the kinetic simulation of chemical ionization in methane oxidation in a shock wave was based on electron concentration profile measurements using a microwave-frequency interferometer. The base methane oxidation mechanism was the kinetic scheme suggested in [14, 15]. This kinetic scheme involves only compounds containing no more than one carbon atom. This was obviously a radical simplification. Nevertheless, this scheme provided a good qualitative agreement between calculated and experimental electron concentration profiles and between the calculated and experimental dependences of the parameters of these profiles on the initial methane concentration and temperature. However, the model needs refinement based on more recent experi-

mental data and on new mechanisms of hydrocarbon oxidation. This refinement is the subject of the present article.

KINETIC MODEL OF IONIZATION

In the description of ionization kinetics in methane oxidation, the methane and ethane oxidation scheme suggested in [19] was used as the base reaction mechanism. This kinetic scheme was formulated by combining the known mechanisms of methane and ethane combustion and was supplemented with data available on reactions involving the components of interest. It accounts well both for the authors' experimental ignition delay data and for literature data in the temperature range from 1200 to 2150 K at pressures of 0.2 to 8 atm. The authors suggest using this scheme in the simulation of methane and ethane combustion.

The methane combustion scheme [19] supplemented with the set of reactions responsible for ionization (reactions 127–138) is presented in Table 1. The rate constants of reverse reactions were calculated using thermochemical data [21, 25]. In this ionization mechanism, the key role is assigned to reactions (I)–(III) (Table 1, reactions 132–134). The set of ionization reactions includes a number of reactions that are missing from the methane combustion scheme but are necessary for the description of CH radical formation and decay (reactions 127–131).

In ionization in shock tubes, some role can be played by impurities. The most important of them are microcrystals of alkali metals, which have a low ionization potential. The fraction of NaCl in a shock tube can reach ~10^{-6} [54], and it is a complicated technical problem to remove this impurity. Note that the initial mixture contains NaCl not as vapor, but as a dispersed solid. However, like Hartig et al. [52], we believe that NaCl evaporates already in the incident shock wave. It was assumed in our calculations that the mixture contains NaCl molecules at a concentration of 10^{12} cm^{-3}. The possible effect of NaCl ionization was taken into account by including reactions 135–138 in the kinetic scheme.

This scheme does not include all reactions possible in the complex ionization process. It is limited to basic reactions playing a significant role in the formation of the electron concentration profile in methane ionization. In the scheme, we ignore many of the ion–molecule reactions involved in the formation of the complicated ionic composition of the mixture. This is done because we did not study the ionic composition experimentally. Furthermore, variations in the ionic composition apparently exert only a minor effect on the electron concentration profile since H_3O^+ still remains the most abundant ion. For these reasons, we will limit our consideration to the reactions yielding the CHO^+ and H_3O^+ ions and some reactions that can help elucidate the role of impurities (NaCl traces).

In the construction of kinetic models for complex chemical reactions, the largest amount of work is usually done to optimize the reaction rate constants (which are either unknown or known with a large uncertainty) so as to attain the best fit between the calculated and observed process parameters. No such optimization is required for the process considered. The rate constants of all of the reactions listed in Table 1 were taken from the literature (see the last column of Table 1), except for reaction 132. The rate constant of this reaction was reduced from 5.6×10^{-13} cm^3/s [18] to 1.5×10^{-13} cm^3/s. Note that the experimental value of this constant is 2.8×10^{-13} cm^3/s [13].

It is significant that the set of reactions 127–138, which supplements the methane combustion scheme, has no sizeable effect on the main oxidation process and is essential only for describing ionization. This was ascertained by calculations.

EXPERIMENTAL

The data calculated for the above-described scheme are compared here with experimental data obtained in our earlier study [57]. In that study, the ionization kinetics of a number of hydrocarbons, including methane, was investigated using a microwave interferometer. The compositions of the mixtures that were used in the study of methane ionization kinetics are listed in Table 2. For each mixture, we indicate the temperature range in which the experiment was performed and the oxygen excess factor (α). The diluent gas was argon. The gas pressure behind the reflected shock wave was 760 ± 150 Torr in all runs. We measured the electron concentration as a function of time, $n_e(t)$, and, from these data, derived the following characteristic parameters of the process: maximum ionization rate (w_{max}), induction period (τ_i), maximum concentration time (τ_{max}), and maximum electron concentration (n_{max}). When comparing experimental data obtained for different mixtures, we replaced the maximum electron concentration with electron yield per methane molecule: $\eta_{max} = n_{max}/n^0_{CH_4}$, where $n^0_{CH_4}$ is the initial methane concentration in the mixture behind the reflected shock wave. In our previous publication [57], the dependences of these parameters on temperature and on the initial methane concentration behind the front of the reflected shock wave were represented as the following relationships:

$$\tau_i = 1.26 \times 10^{-2} (n^0_{CH_4})^{-0.4} \exp(43200/RT), \quad (1)$$

$$\tau_{max} = 0.48 (n^0_{CH_4})^{-0.4} \exp(29900/RT), \quad (2)$$

$$w_{max} = 1.01 \times 10^{6} (n^0_{CH_4})^{1.5} \exp(-34500/RT), \quad (3)$$

$$\eta_{max} = 3.38 \times 10^{2} (n^0_{CH_4})^{-0.4} \exp(-17000/RT) \quad (4)$$

(the activation energies are in cal/mol).

Table 1. Kinetic scheme of ionization in methane combustion*

No.	Reaction	A	n	E_a	Reference
1	$H + O_2 \rightleftarrows O + OH$	5.9×10^{-8}	−0.7	17.1	[20]
2	$H_2 + O \rightleftarrows H + OH$	8.5×10^{-20}	2.67	6.3	[21]
3	$H_2O + O \rightleftarrows OH + OH$	7.6×10^{-15}	1.3	17.1	[22]
4	$H_2O + H \rightleftarrows H_2 + OH$	7.6×10^{-16}	1.6	19.3	[21]
5	$H_2O_2 + OH \rightleftarrows H_2O + HO_2$	2.9×10^{-12}	0	0.3	[22]
6	$H_2O + M \rightleftarrows H + OH + M$	5.8×10^{-9}	0	105.2	[21]
7	$H + O_2 + M \rightleftarrows HO_2 + M$	1.7×10^{-30}	−0.8	0	[21]
8	$HO_2 + O \rightleftarrows OH + O_2$	2.9×10^{-11}	0	−0.4	[22]
9	$HO_2 + H \rightleftarrows OH + OH$	2.8×10^{-10}	0	0.9	[22]
10	$HO_2 + H \rightleftarrows H_2 + O_2$	1.1×10^{-10}	0	2.1	[22]
11	$HO_2 + H \rightleftarrows H_2O + O$	5.0×10^{-11}	0	1.7	[21]
12	$HO_2 + OH \rightleftarrows H_2O + O_2$	2.4×10^{-8}	−1.0	0	[22]
13	$H_2O_2 + M \rightleftarrows OH + OH + M$	3.0×10^{-8}	0	42.9	[21]
14	$H_2O_2 + H \rightleftarrows HO_2 + H_2$	2.8×10^{-12}	0	3.8	[21]
15	$H_2O_2 + O_2 \rightleftarrows HO_2 + HO_2$	8.9×10^{-11}	0	39.7	[22]
16	$H_2O_2 + H \rightleftarrows H_2O + OH$	4.0×10^{-11}	0	4.0	[22]
17	$H_2O_2 + O \rightleftarrows HO_2 + OH$	1.6×10^{-17}	2.0	4.0	[22]
18	$CO + OH \rightleftarrows CO_2 + H$	1.0×10^{-17}	1.5	−0.5	[21]
19	$CO + HO_2 \rightleftarrows CO_2 + OH$	2.5×10^{-10}	0	23.6	[22]
20	$CO + O + M \rightleftarrows CO_2 + M$	1.0×10^{-9}	0	3.0	[22]
21	$CO_2 + O \rightleftarrows CO + O_2$	2.8×10^{-11}	0	52.7	[22]
22	$HCO + M \rightleftarrows H + CO + M$	3.1×10^{-7}	−1.0	17.0	[23]
23	$HCO + OH \rightleftarrows CO + H_2O$	1.7×10^{-10}	0	0	[21]
24	$HCO + H \rightleftarrows CO + H_2$	1.5×10^{-10}	0	0	[21]
25	$HCO + O \rightleftarrows CO + OH$	5.3×10^{-11}	0	0	[21]
26	$HCO + O \rightleftarrows H + CO_2$	5.0×10^{-11}	0	0	[21]
27	$HCO + O_2 \rightleftarrows CO + HO_2$	5.3×10^{-12}	0	0	[21]
28	$HCO + HCO \rightleftarrows CH_2O + CO$	3.0×10^{-11}	0	0	[22]
29	$CH_2O + M \rightleftarrows HCO + H + M$	9.1×10^{-9}	0	75.0	[24]
30	$CH_2O + M \rightleftarrows CO + H_2 + M$	4.2×10^{-8}	0	71.5	[24]
31	$CH_2O + OH \rightleftarrows HCO + H_2O$	5.8×10^{-15}	1.18	−0.4	[21]
32	$CH_2O + H \rightleftarrows HCO + H_2$	3.8×10^{-14}	1.05	3.3	[21]
33	$CH_2O + O \rightleftarrows HCO + OH$	6.9×10^{-13}	0.57	2.8	[21]
34	$CH_2O + O_2 \rightleftarrows HCO + HO_2$	3.4×10^{-11}	0	39.0	[22]
35	$CH_2O + HO_2 \rightleftarrows HCO + H_2O_2$	3.3×10^{-12}	0	11.7	[22]
36	$CH_2O + CH_3 \rightleftarrows CH_4 + HCO$	9.1×10^{-21}	2.81	5.9	[22]
37	$CH_4 \rightleftarrows CH_3 + H$	4.0×10^{14}	0	105.7	[25]**
38	$CH_4 + H \rightleftarrows CH_3 + H_2$	2.2×10^{-20}	3.0	8.0	[21]
39	$CH_4 + OH \rightleftarrows CH_3 + H_2O$	2.6×10^{-17}	1.83	2.8	[21]
40	$CH_4 + O \rightleftarrows CH_3 + OH$	1.1×10^{-15}	1.56	8.5	[21]
41	$CH_4 + CH \rightleftarrows C_2H_4 + H$	1.0×10^{-10}	0	0	[25]
42	$CH_4 + O_2 \rightleftarrows CH_3 + HO_2$	6.6×10^{-11}	0	56.9	[21]
43	$CH_4 + CH_2 \rightleftarrows CH_3 + CH_3$	3.0×10^{-10}	0	14.4	[26]
44	$CH_4 + HO_2 \rightleftarrows CH_3 + H_2O_2$	1.5×10^{-11}	0	24.6	[21]
45	$CH_3 + M \rightleftarrows CH_2 + H + M$	3.2×10^{-8}	0	91.4	[27]
46	$CH_3 + M \rightleftarrows CH + H_2 + M$	1.7×10^{-8}	0	85.3	[28]
47	$CH_3 + HO_2 \rightleftarrows CH_3O + OH$	3.0×10^{-11}	0	0	[21]

Table 1. (Contd.)

No.	Reaction	A	n	E_a	Reference
48	$CH_3 + OH \rightleftarrows CH_2O + H_2$	5.3×10^{-12}	–0.53	10.8	[29]
49	$CH_3 + OH \rightleftarrows CH_2 + H_2O$	2.5×10^{-11}	0	5.0	[30]
50	$CH_3 + OH \rightleftarrows CH_3O + H$	9.6×10^{-12}	–0.23	13.9	[29]
51	$CH_3 + OH \rightleftarrows CH_2OH + H$	4.4×10^{-5}	–1.8	8.1	[29]
52	$CH_3 + O \rightleftarrows CH_2O + H$	1.4×10^{-10}	0	0	[21]
53	$CH_3 + O_2 \rightleftarrows CH_3O + O$	3.8×10^{-11}	0	30.6	[31]
54	$CH_3 + O_2 \rightleftarrows CH_2O + OH$	5.5×10^{-13}	0	8.9	[21]
55	$CH_3 + HCO \rightleftarrows CH_4 + CO$	2.0×10^{-10}	0	0	[22]
56	$CH_3 + H \rightleftarrows CH_2 + H_2$	1.0×10^{-10}	0	15.1	[21]
57	$CH_3 + CH_2 \rightleftarrows C_2H_4 + H$	6.9×10^{-11}	0	0	[21]
58	$CH_3 + CH_3 \rightleftarrows C_2H_5 + H$	5.3×10^{-11}	0	13.5	[21]
59	$CH_3O + M \rightleftarrows CH_2O + H + M$	8.9×10^{-11}	0	13.5	[32]
60	$C_2H_6 \rightleftarrows CH_3 + CH_3$	1.0×10^{16}	0	87.9	[33]**
61	$C_2H_6 \rightleftarrows C_2H_5 + H$	1.1×10^{16}	0	98.1	[33]**
62	$C_2H_6 + CH_3 \rightleftarrows C_2H_5 + CH_4$	2.6×10^{-31}	6.0	6.1	[21]
63	$C_2H_6 + H \rightleftarrows C_2H_5 + H_2$	2.4×10^{-15}	1.5	7.4	[21]
64	$C_2H_6 + OH \rightleftarrows C_2H_5 + H_2O$	1.2×10^{-17}	2.0	0.9	[21]
65	$C_2H_6 + O \rightleftarrows C_2H_5 + OH$	1.7×10^{-15}	1.5	5.8	[21]
66	$C_2H_6 + O_2 \rightleftarrows C_2H_5 + HO_2$	1.0×10^{-10}	0	51.9	[21]
67	$C_2H_6 + HO_2 \rightleftarrows C_2H_5 + H_2O_2$	2.2×10^{-11}	0	20.5	[21]
68	$C_2H_5 \rightleftarrows C_2H_4 + H$	5.0×10^{13}	0	40.9	[34]
69	$C_2H_5 + O \rightleftarrows CH_3CHO + H$	1.3×10^{-10}	0	0	[22]
70	$C_2H_5 + O \rightleftarrows CH_2O + CH_3$	2.7×10^{-11}	0	0	[22]
71	$C_2H_5 + H \rightleftarrows C_2H_4 + H_2$	3.0×10^{-12}	0	0	[22]
72	$C_2H_5 + O_2 \rightleftarrows C_2H_4 + HO_2$	1.4×10^{-12}	0	3.9	[22]
73	$C_2H_5 + O_2 \rightleftarrows CH_3CH_2O + O$	1.9×10^{-11}	–0.2	27.93	[35]
74	$C_2H_5 + HO_2 \rightleftarrows C_2H_4 + H_2O_2$	5.3×10^{-13}	0	0	[22]
75	$C_2H_5 + OH \rightleftarrows C_2H_4 + H_2O$	4.2×10^{-11}	0	0	[22]
76	$C_2H_4 + M \rightleftarrows C_2H_2 + H_2 + M$	5.8×10^{-8}	0	71.5	[25]
77	$C_2H_4 + M \rightleftarrows C_2H_3 + H + M$	4.3×10^{-7}	0	96.6	[25]
78	$C_2H_4 + O \rightleftarrows CH_3 + HCO$	2.2×10^{-16}	1.55	0.6	[22]
79	$C_2H_4 + O \rightleftarrows C_2H_3 + OH$	6.6×10^{-10}	0	18.9	[36]
80	$C_2H_4 + O \rightleftarrows CH_3CO + H$	5.8×10^{-11}	0	2.8	[36]
81	$C_2H_4 + O \rightleftarrows CH_2 + CH_2O$	3.0×10^{-11}	0	4.0	[33]
82	$C_2H_4 + H \rightleftarrows C_2H_3 + H_2$	8.9×10^{-10}	0	14.9	[21]
83	$C_2H_4 + OH \rightleftarrows C_2H_3 + H_2O$	3.4×10^{-11}	0	5.9	[21]
84	$C_2H_4 + HO_2 \rightleftarrows CH_3CHO + OH$	1.0×10^{-14}	0	7.9	[22]
85	$C_2H_4 + CH_3 \rightleftarrows CH_4 + C_2H_3$	2.2×10^{-11}	0	11.1	[21]
86	$C_2H_3 + M \rightleftarrows C_2H_2 + H + M$	6.9×10^{17}	–7.5	45.5	[21]
87	$C_2H_3 + O \rightleftarrows CH_2CO + H$	1.6×10^{-10}	0	0	[22]
88	$C_2H_3 + H \rightleftarrows C_2H_2 + H_2$	2.0×10^{-11}	0	0	[21]
89	$C_2H_3 + OH \rightleftarrows C_2H_2 + H_2O$	5.3×10^{-11}	0	0	[22]
90	$C_2H_3 + O_2 \rightleftarrows C_2H_2 + HO_2$	2.0×10^{-13}	0	0	[22]
91	$C_2H_3 + O_2 \rightleftarrows CH_2O + HCO$	8.9×10^{-12}	0	0	[21]
92	$C_2H_3 + CH_3 \rightleftarrows C_2H_2 + CH_4$	3.3×10^{-11}	0	0	[37]
93	$C_2H_2 + OH \rightleftarrows C_2H + H_2O$	2.4×10^{-20}	2.68	12.0	[22]
94	$C_2H_2 + OH \rightleftarrows CH_3 + CO$	7.9×10^{-28}	4.0	–2.0	[38]

Table 1. (Contd.)

No.	Reaction	A	n	E_a	Reference
95	$C_2H_2 + OH \rightleftharpoons CH_2CO + H$	3.6×10^{-28}	4.5	–1	[38]
96	$C_2H_2 + O \rightleftharpoons HCCO + H$	6.6×10^{-10}	0	10.7	[39]
97	$C_2H_2 + O \rightleftharpoons CH_2 + CO$	2.6×10^{-10}	0	9.9	[39]
98	$C_2H_2 + O \rightleftharpoons C_2H + OH$	6.6×10^{-9}	–0.6	15.0	[40]
99	$CH_2 + O_2 \rightleftharpoons HCO + OH$	2.8×10^{-3}	–3.3	2.9	[41]
100	$CH_2 + O_2 \rightleftharpoons CO_2 + H + H$	5.5×10^{-2}	–3.3	2.9	[41]
101	$CH_2 + O_2 \rightleftharpoons CO + H_2O$	3.7×10^{-2}	–3.3	2.9	[41]
102	$CH_2 + O \rightleftharpoons CO + H + H$	1.0×10^{-10}	0	0	[21]
103	$CH_2 + OH \rightleftharpoons CH_2O + H$	3.0×10^{-11}	0	0	[22]
104	$CH + O_2 \rightleftharpoons CO + OH$	8.3×10^{-11}	0	0	[42]
105	$CH_3OH + M \rightleftharpoons CH_3 + OH + M$	1.1×10^{-7}	0	65.7	[25]
106	$CH_3OH + OH \rightleftharpoons CH_2OH + H_2O$	2.4×10^{-18}	2.0	–0.8	[43]
107	$CH_3OH + OH \rightleftharpoons CH_3O + H_2O$	6.0×10^{-13}	0.7	5.9	[44]
108	$CH_3OH + O \rightleftharpoons CH_2OH + OH$	5.8×10^{-11}	0	5.5	[45]
109	$CH_3OH + H \rightleftharpoons CH_2OH + H_2$	5.6×10^{-11}	0	2.6	[43]
110	$CH_3OH + H \rightleftharpoons CH_3 + H_2O$	3.3×10^{-10}	0	5.3	[46]
111	$CH_2OH + M \rightleftharpoons CH_2O + H + M$	7.2×10^{-9}	0	30	[46]
112	$CH_2OH + O_2 \rightleftharpoons CH_2O + HO_2$	2.0×10^{-12}	0	0	[47]
113	$CH_3CHO \rightleftharpoons CH_3 + HCO$	1.2×10^{-8}	0	81.7	[22]
114	$CH_3CHO + H \rightleftharpoons CH_3CO + H_2$	6.8×10^{-15}	1.16	2.4	[21]
115	$CH_3CHO + OH \rightleftharpoons CH_3CO + H_2O$	5.6×10^{-12}	0	–0.6	[21]
116	$CH_3CO + M \rightleftharpoons CH_3 + CO + M$	1.4×10^{19}	–8.62	22.4	[22]
117	$CH_3CO + OH \rightleftharpoons CH_2CO + H_2O$	2.0×10^{-11}	0	0	[22]
118	$CH_3CO + H \rightleftharpoons CH_2CO + H_2$	1.7×10^{-11}	0	0	[48]
119	$CH_2CO + H \rightleftharpoons CH_3 + CO$	3.0×10^{-11}	0	0	[49]
120	$CH_2CO + H \rightleftharpoons HCCO + H_2$	3.0×10^{-10}	0	8.6	[33]
121	$CH_2CO + OH \rightleftharpoons CH_2OH + CO$	8.3×10^{-12}	0	0	[33]
122	$HCCO + M \rightleftharpoons CH + CO + M$	1.1×10^{-8}	0	58.8	[39]
123	$HCCO + OH \rightleftharpoons H_2O + C_2O$	5.3×10^{-11}	0	0	[26]
124	$HCCO + OH \rightleftharpoons CO + CO + H_2$	1.7×10^{-10}	0	0	[33]
125	$HCCO + O \rightleftharpoons CO + CO + H$	1.6×10^{-10}	0	0	[21]
126	$HCCO + H \rightleftharpoons CH_2 + CO$	2.5×10^{-10}	0	0	[39]
127	$CH_2 + O \longrightarrow CH + OH$	5.0×10^{-10}	0	11.9	[25]
128	$CH_2 + OH \longrightarrow CH + H_2O$	1.7×10^{-11}	0	0	[13]
129	$CH_2 + H \rightleftharpoons CH + H_2$	2.34×10^{-10}	0	0	[29]
130	$CH + O_2 \longrightarrow CO + OH$	8.32×10^{-11}	0	0	[13]
131	$CH + O_2 \longrightarrow CHO + O$	1.66×10^{-11}	0	0	[50]
132	$CH + O \rightleftharpoons CHO^+ + e^-$	1.5×10^{-13}	0	0	[13]
133	$CHO^+ + H_2O \rightleftharpoons H_3O^+ + CO$	1.5×10^{-8}	0	0	[18]
134	$H_3O^+ + e \longrightarrow H_2O + H$	7.6×10^{-2}	–1.6	0	[11, 51]
135	$NaCl + M \longrightarrow Na + Cl + M$	8.3×10^{-10}	0	80	[52]
136	$Na + M \longrightarrow Na^+ + e + M$	3.1×10^{-9}	0.5	118.0	[53]
137	$NaCl + M \longrightarrow Na^+ + Cl^- + M$	8.2×10^{-2}	–2.0	134.0	[54]
138	$H_3O^+ + Na \longrightarrow Na^+ + H_2O + H$	1.1×10^{-8}	0	0	[55]

* The rate constants are represented as $k = AT^n\exp(-E_a/RT)$. The dimension of the preexponential factor A is cm^3 s, and the dimension of the activation energy E_a is kcal/mol.
** The rate constants of the monomolecular reactions in the transition pressure range were calculated using the procedure presented in [56].

Table 2. Compositions of the mixtures examined in ionization kinetic experiments

Mixture number	$[CH_4]$, %	$[O_2]$, %	T, K	α
1	0.75	3.0	2200–2850	2.0
2	0.5	2.0	2170–3140	2.0
3	0.2	0.8	2500–3000	2.0
4	0.5	1.5	1980–3100	1.5

CALCULATED IONIZATION KINETICS

Ionization was numerically simulated for the four mixtures listed in Table 2 at temperatures of 1900 to 3200 K. For the sake of demonstrativeness, the calculations were carried out for the same conditions as in particular runs. In Fig. 1, the experimental electron concentration profiles obtained near 2250, 2500, and 2750 K are compared with the profiles calculated for the same conditions. (For brevity, just these temperatures, which differ from the true temperatures by 10–20 K, are indicated in the caption to Fig. 1.)

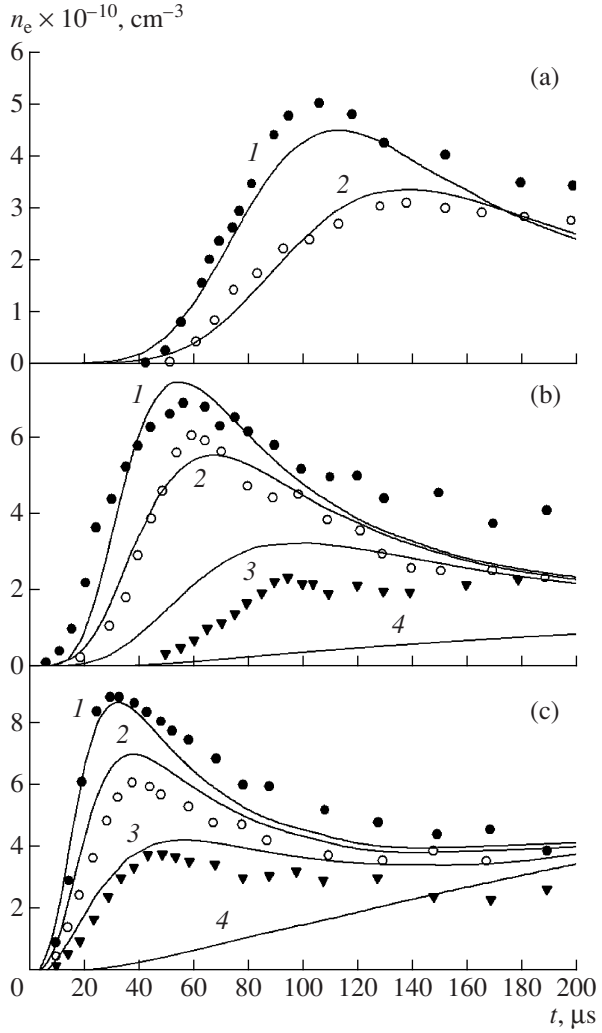

Fig. 1. Electron concentration profiles at (a) 2250, (b) 2500, and (c) 2750 K for mixtures (*1*) 1, (*2*) 2, and (*3*) 3. The points represent experimental data, and the solid lines represent calculated data. (*4*) Calculated Na^+ concentration.

The kinetic curves calculated for mixture 2 at T = 2740 K are plotted in Figs. 2 and 3. Figure 2 presents the calculated concentration profiles for the most abundant neutral species—CH_4, CH_3, CH_2, CH, O_2, and O—and the calculated time dependence of the ionization rate (w). The concentrations of the radicals CH_3, CH_2, and CH successively reach their maximum values, which are 3.30×10^{15}, 9.00×10^{13}, and 1.35×10^{13} cm^{-3} at t = 4.5, 8.0, and 10.5 μs, respectively. The highest ionization rate, $w_{max} = 5.8 \times 10^{15}$ cm^{-3} s^{-1}, is reached at t = 20 μs. Under these conditions, the conversion of the initial compound is almost complete in 50 μs. By this point in time, the ionization rate decreases by one order of magnitude relative to its maximum, indicating that chemical ionization is also complete.

Figure 3 shows the concentration profiles of the main charged species—CHO^+, H_3O^+, and Na^+ ions and electrons—and the time dependence of the ionization rate calculated for mixture 2 and the corresponding experimental electron concentration curve. Clearly, the CHO^+ ion forms first, whose concentration peaks in 8 μs, earlier than the concentrations of the other ions. However, because of rapid recharging yielding H_3O^+, the CHO^+ concentration is not high, its maximum value being 8.7×10^8 cm^{-3}. The concentration of H_3O^+ ions, whose maximum formation rate is 7.0×10^{16} cm^{-3} s^{-1} and coincides in time with the CHO^+ concentration peak, reaches its maximum value of 9.3×10^{10} cm^{-3} at t = 40 μs. The fact that the H_3O^+ formation rate is nearly one order of magnitude higher than the ionization rate is explained by the occurrence of the rapid reverse reaction.

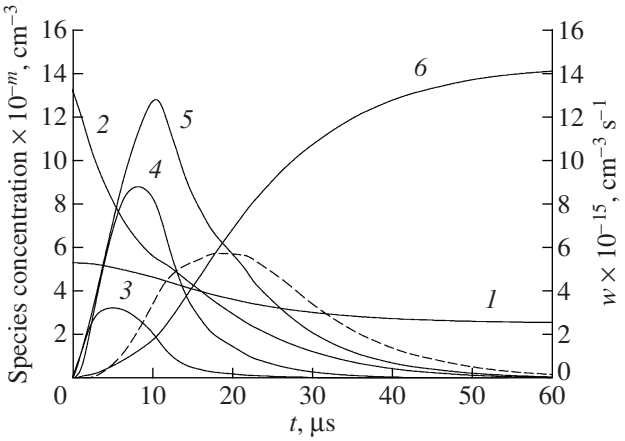

Fig. 2. Calculated profiles of the neutral species concentration and ionization rate (dashed line) at T = 2740 K for mixture 2: (*1*) O_2 (m = 16), (*2*) CH_4 (m = 15), (*3*) CH_3 (m = 15), (*4*) CH_2 (m = 13), (*5*) CH (m = 12), and (*6*) O atom (m = 15).

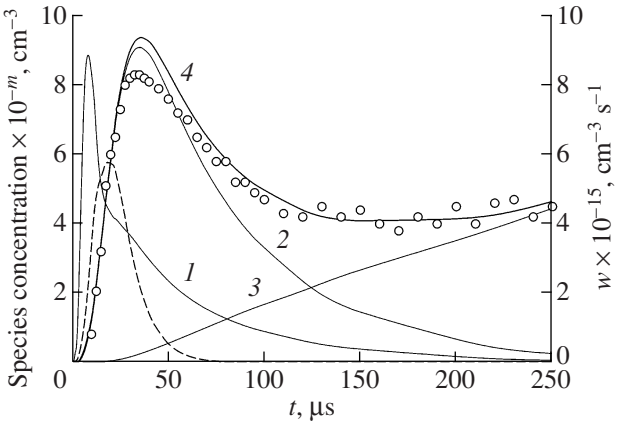

Fig. 3. (*1–3*) Calculated concentration profiles for charged particles and (*4*) ($m = 10$) experimental electron concentration profile for mixture 2 at $T = 2740$ K: (*1*) CHO^+ ($m = 8$), (*2*) H_3O^+ ($m = 10$), and (*3*) Na^+ ($m = 10$). The dashed line is the ionization rate at $T = 2740$ K.

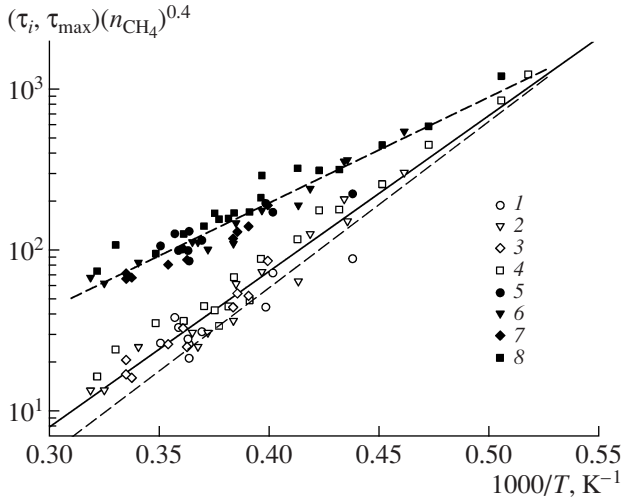

Fig. 4. Experimental temperature dependences of (*1–4*) the induction period of ionization and (*5–8*) the maximum electron concentration time for methane oxidation in mixtures (*1*, *5*) 1, (*2*, *6*) 2, (*3*, *7*) 3, and (*4*, *8*) 4. The solid line is the plot of relationship (1), and the dashed line represents the data calculated using the kinetic scheme.

At the point of maximum electron concentration, the Na^+ concentration is 2.9×10^9 cm^{-3}, which is more than one order of magnitude lower than the H_3O^+ concentration. Due to this circumstance, the electron and ion concentration peaks are nearly equal in magnitude and almost coincide in time.

After passing through the maximum, the H_3O^+ concentration begins to decrease mainly because of the recombination reaction (III). As this takes place, the concentration of Na^+ ions, which form at a rate of $\sim 2 \times 10^{14}$ cm^{-3} s^{-1}, gradually increases to become comparable with the highest H_3O^+ concentration. For example, at $t = 200$ μs, the Na^+ concentration is 3.6×10^{10} cm^{-3}. As a consequence, the electron concentration, gradually decreasing from its maximum value, passes through a minimum (4.2×10^{10} cm^{-3}) at $t = 150$ μs and begins to grow again, tending to its equilibrium value. Note that, under the given conditions, the equilibrium electron concentration is determined primarily by the presence of sodium in the mixture and is $\sim 2.5 \times 10^{11}$ cm^{-3}.

The calculated electron concentration profiles were processed in the same way as the experimental profiles to determine the maximum ionization rate w_{max}, the induction period τ_i, the maximum electron concentration time τ_{max}, and the maximum electron concentration n_{max}. In Figs. 4–6, the dashed lines represent the calculated temperature dependences of the process parameters and are compared with experimental data. The solid lines represent relationships (1)–(4). Clearly, all of the calculated dependences differ insignificantly from their experimental counterparts and the discrepancy does not exceed the spread of the experimental data. The calculated temperature dependence of the maximum electron concentration time almost coincides with the corresponding experimental dependence.

RESULTS AND DISCUSSION

The calculations revealed the following features of the development of the process:

(1) At the initial stage of the process, electrons result almost solely from reaction (I) (no. 132 in Table 1).

(2) The resulting CHO^+ ion reacts rapidly with water (reaction (II), no. 133 in Table 1). This yields the H_3O^+ ion, which is the most abundant at the initial stage of the process.

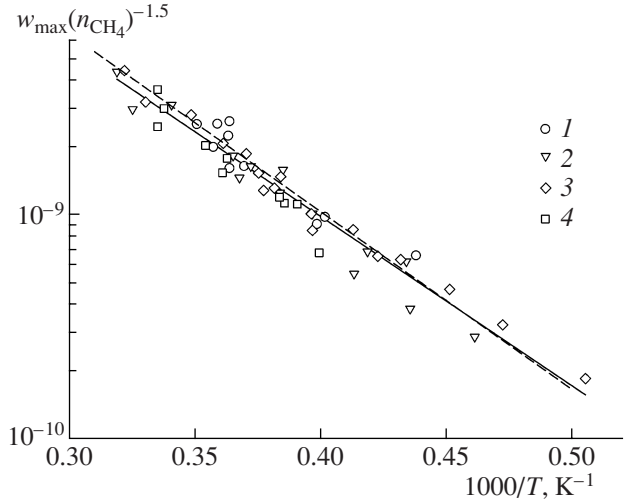

Fig. 5. Experimental temperature dependences of the ionization rate for methane oxidation in mixtures (*1*) 1, (*2*) 2, (*3*) 3, and (*4*) 4. The solid line is the plot of relationship (4), and the dashed line represents the data calculated using the kinetic scheme.

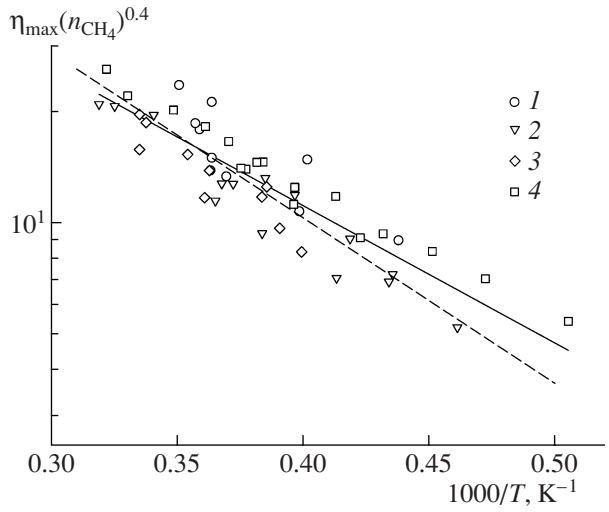

Fig. 6. Experimental temperature dependences of the electron yield for methane oxidation in mixtures (*1*) 1, (*2*) 2, (*3*) 3, and (*4*) 4. The solid line is the plot of relationship (4), and the dashed line represents the data calculated using the kinetic scheme.

(3) The electron concentration maximum almost coincides in time with, and is approximately equal in magnitude to, the H_3O^+ concentration peak.

(4) The maximum electron concentration time nearly coincides with completion of the chemical conversion of the initial reactant (methane).

(5) After passing through the maximum, the electron concentration falls to some minimum value because of recombination and then begins to increase owing to the continuing ionization of sodium.

The results of the numerical calculations of chemical ionization in methane oxidation provide a qualitative description for the time variation of the electron concentration. They confirm the existing view that the primary ionization event in hydrocarbon combustion is the associative ionization reaction (I). The calculated dependences of the parameters of the electron concentration profile on temperature and on the initial methane concentration in the mixture are close to the corresponding experimental dependences. Among the hydrocarbon oxidation processes, high-temperature methane oxidation has been investigated most extensively. Its mechanism is understood most comprehensively and is widely used in numerical simulation of various combustion processes involving saturated hydrocarbons. Although the base methane oxidation scheme used in this study was intended for describing ignition delay data [19], it was successfully used for another process in a much wider temperature range (for the late stages of the process). This points to the high reliability of the numerous earlier studies that dealt with the set of reactions necessary for describing methane combustion and with the rate constants of these reactions.

In the description of the late stages of ionization in shock waves, when a secondary increase in the electron concentration takes place, we used the concept of impurity (sodium salt) ionization. This process or a similar one definitely occurs in shock waves, as is evident from the data available on impurities in shock tubes [52]. However, we cannot claim with absolute certainty that it is this process that dominates at the stage of the secondary electron concentration rise. Other processes are also possible, including processes that involve pump oil, which are more difficult to take into account. Nevertheless, it is clear that the secondary increase in the electron concentration is independent of ionization associated with methane oxidation, because it begins after methane is completely burnt. It can be stated that the chemical ionization wave, which is characterized by an electron concentration peak, is followed by an impurity ionization wave, which is most likely due to the thermal ionization of sodium.

Thus, from the good qualitative agreement between the calculated and observed electron concentration profiles and from the coincidence between the calculated and observed dependences of the parameters of these profiles on temperature and on the initial methane concentration, we infer that the present-day notion of combustion kinetics and ionization in hydrocarbons provides a correct description of this process. Since there are some discrepancies between the experimental and calculated characteristics of ionization, the kinetic model of hydrocarbon combustion needs further refinement. Therefore, kinetic studies of combustion-induced ionization are a helpful extra source of information about hydrocarbon combustion and thus contribute to the fundamental knowledge of this process.

REFERENCES

1. Aravin, G.S., *Cand. Sci. (Phys.–Math.) Dissertation*, Moscow: Inst. of Chemical Physics, 1951.
2. Calcott, H.F., *3rd Int. Symp. on Combustion*, Pittsburgh: The Combustion Inst., 1949, p. 245.
3. De Jgaegere, S., Deckers, J., and van Tiggelen, A., *8th Int. Symp. on Combustion*, Pittsburgh: The Combustion Inst.,1962, p. 155.
4. Calcotte, H.F. and Reuter, J.L., *J. Chem. Phys.*, 1963, vol. 38, p. 310.
5. Calcotte, H.F., *8th Int. Symp. on Combustion*, Pittsburgh: The Combustion Inst.,1962, p. 184.
6. Miller, M.J., *14th Int. Symp. on Combustion*, Pittsburgh: The Combustion Inst.,1973, p. 307.
7. Matthews, C.S. and Warneck, P., *J. Chem. Phys.*, 1959, vol. 51, no. 5, p. 854.
8. Peeters, J. and van Tiggelen, A., *12th Int. Symp. on Combustion*, Pittsburgh: The Combustion Inst., 1969, p. 437.
9. Betowski, D., Payzant, J.D., Mackay, G.I., and Bohme, D.K., *Chem. Phys. Lett.*, 1975, vol. 31, no. 2, p. 321.
10. Ko, S., *Combust. Flame*, 1973, vol. 21, no. 1, p. 241.

11. Hayhurst, A.N. and Telford, N.R., *J. Chem. Soc., Faraday Trans.*, 1974, no. 11, p. 181.
12. MacGregor, M. and Barry, R.S., *J. Phys. B: At., Mol. Opt. Phys.*, 1973, vol. 6, no. 1, p. 181.
13. Peeters, J. and Vinckier, C., *15th Int. Symp. on Combustion*, Pittsburgh: The Combustion Inst., 1974, p. 969.
14. Basevich, V.Ya., Kogarko, S.M., and Furman, G.A., *Izv. Akad. Nauk SSSR, Ser. Khim.*, 1974, vol. 1, no. 2, p. 197.
15. Basevich, V.Ya., Kogarko, S.M., and Furman, G.A, *Izv. Akad. Nauk SSSR, Ser. Khim.*, 1971, vol. 7, no. 11, p. 1406.
16. Semenov, E.S. and Sokolik, A.S., *Zh. Tekh. Fiz.*, 1962, vol. 32, no. 6, p. 1074.
17. Lester, T.W., Zallen, D.M., and Vittig, S.L.K., *Combust. Sci. Technol.*, 1973, vol. 7, no. 1, p. 219.
18. Aravin, G.S., Vlasov, P.A., Karasevich, Yu.K., Makolkin, E.V., and Neigauz, M.G., *Fiz. Goreniya Vzryva*, 1982, no. 1, p. 49.
19. Tereza, A.M., Slutskii, V.G., and Severin, E.S., *Khim. Fiz.*, 2003, vol. 22, no. 6, p. 30.
20. Masten, D.A., Hanson, R.K., and Bowman, C.T., *J. Phys. Chem.*, 1990, vol. 94, p. 7119.
21. Baulch, D.L., Cobos, C.J., Cox, R.A., et al., *J. Phys. Chem. Ref. Data*, 1992, vol. 21, p. 411.
22. Tsang, W. and Hampson, R.F., *J. Phys. Chem. Ref. Data*, 1986, vol. 15, p. 1087.
23. Timonen, R.S., Ratajczak, E., Gutman, D., and Wagner, A.F., *J. Phys. Chem.*, 1987, vol. 91, p. 5325.
24. Hidaka, Y., Taniguchi, T., Tanaka, H., Kamesawa, T., Inami, K., and Kawano, H., *Combust. Flame*, 1993, vol. 92, p. 365.
25. Baulch, D.L., Cobos, C.J., Cox, R.A., et al., *J. Phys. Chem. Ref. Data*, 1994, vol. 23, p. 847.
26. Wang, H. and Frenklach, M., *Combust. Flame*, 1997, vol. 110, p. 173.
27. Zborovskii, A.G., Petrov, Yu.P., Tereza, A.M., and Tyurin, A.N., *Khim. Fiz.*, 1990, vol. 5, no. 11, p. 1528.
28. Markus, M.W., Woiki, D., and Roth, P., *24th Int. Symp. on Combustion*, Pittsburgh: The Combustion Inst., 1992, p. 581.
29. Rohrig, M., Petersen, E.L., Davidson, D.F., Hanson, R.K., and Bowman, C.T., *Int. J. Chem. Kinet.*, 1997, vol. 29, p. 81.
30. Dean, A.M. and Westmoreland, P.R., *Int. J. Chem. Kinet.*, 1987, vol. 19, p. 207.
31. Glarborg, F., Miller, J.A., and Kee, R.J., *Combust. Flame*, 1986, vol. 65, p. 177.
32. Klatt, M., Rohrig, M., and Wagner, H.Gg., *Ber. Bunsen-Ges. Phys. Chem*, 1991, vol. 95, p. 1163.
33. Hidaka, Y., Nishimori, T., Sato, K., Henmi, Y., Okuda, R., and Inami, K., *Combust. Flame*, 1999, vol. 117, p. 755.
34. Dean, A.M., *J. Phys. Chem.*, 1985, vol. 89, p. 4600.
35. Bozzelli, J.W. and Dean, A.M., *J. Phys. Chem.*, 1990, vol. 94, p. 3313.
36. Frank, P. and Just, Th., *Proc. Int. Symp. on Shock Tubes and Waves*, Sydney, 1984, vol. 14, p. 706.
37. Fahr, A., Laufer, A., Klein, R., and Braun, W., *J. Phys. Chem.*, 1991, vol. 95, p. 3218.
38. Miller, J.A. and Melius, C.F., *Int. Symp. on Combustion Processes*, 1989, vol. 22, p. 1031.
39. Frank, P. and Just, Th., *Proc. Int. Symp. on Shock Tubes and Waves*, Sydney, 1984, vol. 14, p. 706.
40. Miller, J.A., Mitchell, R.E., Smooke, M.D., et al., *19th Int. Symp. on Combustion*, Pittsburgh: The Combustion Inst., 1982, p. 181.
41. Dombrowsky, Ch. and Wagner, H.Gg., *Ber. Bunsen-Ges. Chem.*, 1992, vol. 96, p. 1048.
42. Lichtin, D.A., Berman, M.R., and Lin, M.C., *Chem. Phys. Lett.*, 1984, vol. 108, p. 18.
43. Li, S.C. and Williams, F.A., *26th Int. Symp. on Combustion*, Pittsburgh: The Combustion Inst., 1996, p. 1017.
44. Degaut, P., Boettner, J.C., and Cathonnet, M., *Combust. Sci. Technol.*, 1991, vol. 77, p. 127.
45. Failes, R.L., Singleton, D.L., Paraskevopoulos, G., and Irwin, R.S., *Int. J. Chem. Kinet.*, 1982, vol. 14, p. 371.
46. Hidaka, Y., Oki, T., and Kawano, H., *J. Phys. Chem.*, 1989, vol. 93, p. 7134.
47. Tsang, W., *J. Phys. Chem. Ref. Data*, 1987, vol. 16, p. 471.
48. Bartels, M., Edelbuttel-Einhaus, J., and Hoyermann, K., *23rd Int. Symp. on Combustion*, Pittsburgh: The Combustion Inst., 1990, p. 131.
49. Frank, P., Bhaskaran, K.A., and Just, Th., *J. Phys. Chem.*, 1986, vol. 90, p. 2226.
50. Jachimowski, C.J., *Combust. Flame*, 1977, vol. 29, no. 1, p. 55.
51. Kelly, R. and Padly, P.J., *Trans. Faraday Soc.*, 1970, vol. 66, no. 5, p. 1127.
52. Hartig, R., Olschewski, H.A., Troe, J., and Wagner, H.Gg., *Ber. Bunsen-Ges. Phys. Chem.*, 1968, vol. 72, no. 8, p. 1016.
53. Bates, D.R., *Proc. R. Soc. London, Ser. A*, 1976, vol. 348, no. 1655, p. 427.
54. Schneider, K.P. and Park, C., *Phys. Fluids*, 1975, vol. 18, no. 5, p. 969.
55. Hayhurst, N.A. and Sugden, T.M., *Proc. R. Soc. London, Ser. A*, 1966, vol. 293, no. 1600, p. 36.
56. Bakulina, G.V., Bespalov, E.V., Kazakov, O.D., Severin, E.S., Slutskii, V.G., Tereza, A.M., and Tsyganov, S.A., *Khim. Fiz.*, 1991, vol. 10, no. 3, p. 407.
57. Karasevich, Yu.K., *Kinet. Katal.*, 2008, vol. 49, no. 5, p. 640 [*Kinet. Catal.* (Engl. Transl.), vol. 49, no. 5, p. 610].